

Phase equilibria in the system CaO-CoO-SiO₂ and Gibbs energies of formation of the quaternary oxides CaCoSi₂O₆, Ca₂CoSi₂O₇, and CaCoSiO₄

SUKANYA MUKHOPADHYAY AND K.T. JACOB

Department of Metallurgy, Indian Institute of Science, Bangalore 560 012, India

ABSTRACT

Phase relations in the pseudoternary system CaO-CoO-SiO₂ have been established at 1323 K. Three quaternary oxides were found to be stable: CaCoSi₂O₆ with clinopyroxene (Cpx), Ca₂CoSi₂O₇ with melilite (Mel), and CaCoSiO₄ with olivine (Ol) structures. The Gibbs energies of formation of the quaternary oxides from their component binary oxides were measured using solid-state galvanic cells incorporating yttria-stabilized zirconia as the solid electrolyte in the temperature range of 1000–1324 K. The results can be summarized as follows:



$$\Delta G_f^\circ = -117920 + 11.26T (\pm 150) \text{ J/mol}$$



$$\Delta G_f^\circ = -192690 + 2.38T (\pm 130) \text{ J/mol}$$



$$\Delta G_f^\circ = -100325 + 2.55T (\pm 100) \text{ J/mol}$$

where rs = rock salt (NaCl) structure and Qtz = quartz. The uncertainty limits correspond to twice the standard error estimate.

The experimentally observed miscibility gaps along the joins CaO-CoO and CaCoSiO₄-Co₂SiO₄ were used to calculate the excess free energies of mixing for the solid solutions Ca_xCo_{1-x}O and (Ca_YCo_{1-Y})CoSiO₄: $\Delta G^E = X(1 - X)[31975X + 26736(1 - X)]$ J/mol and $\Delta G^E = 23100 (\pm 250) Y(1 - Y)$ J/mol. A *T*-*X* phase diagram for the binary CaO-CoO was computed from the thermodynamic information; the diagram agrees with information available in the literature. The computed miscibility gap along the CaCoSiO₄-Co₂SiO₄ join is associated with a critical temperature of 1389 (±15) K. Stability fields for the various solid solutions and the quaternary compounds are depicted on chemical-potential diagrams for SiO₂, CaO, and CoO at 1323 K.

INTRODUCTION

Kinetic demixing of homogeneous solid solutions and kinetic decomposition of ternary and higher order compounds in generalized thermodynamic potential gradients (Schmalzried et al. 1979; Jacob 1983; Ishikawa et al. 1985; Jacob and Shukla 1987; Shukla and Jacob 1987) are important phenomena with major implications for the evolution of mineralogic structures. To understand these complex phenomena, it is convenient to study multicomponent model systems in which one or more parameters are kept invariant. The system Co-Mg-Ca-Si-O was selected for investigation of the unknown phase equilibria and thermodynamic properties at high temperature. These silicates do not exhibit O nonstoichiometry.

This study establishes a complete isothermal section of the phase diagram for the system at 1323 K and determines the thermodynamic properties of the quaternary phases and solid solutions at high temperature. These data are of interest in mineralogy, metallurgy, and ceramics. They provide an insight into the topology of phase relations in analogous, but more complex, pyroxene-melilite-olivine mineralogic systems.

Four quaternary silicates, CaCoSi₂O₆, Ca₂CoSi₂O₇, CaCoSiO₄, and CaCoSi₄O₁₀, have been reported in the literature in the pseudoternary system CaO-CoO-SiO₂. The crystal chemistry of the clinopyroxene CaCoSi₂O₆, with *C2/c* symmetry, has been studied by Ghose and Wan (1975) and Ghose et al. (1987). The study of transition-metal bearing pyroxenes is of interest from the point

of view of providing a fundamental understanding of the relationships among crystal structure, chemical bonding, magnetic properties, thermodynamics, and phase relations. Navrotsky and Coons (1976) determined the enthalpy of formation of CaCoSi₂O₆ from the oxides at 986 K using oxide-melt solution calorimetry. Information on the Gibbs energy of formation of CaCoSi₂O₆ is not available.

Ca₂CoSi₂O₇, with a melilite structure was synthesized by Brisi and Abbattista (1960) and crystallizes in the tetragonal system with unit-cell parameters $a = 0.786$ and $c = 0.503$ nm. CaCoSiO₄, with an olivine structure, space group *Pnma*, $a = 0.4827$, $b = 1.112$, and $c = 0.6406$ nm, was prepared by Newnham et al. (1966). Nicolini and Porta (1970) identified the quaternary compound CaCoSi₄O₁₀, which crystallizes in the tetragonal *P4/ncc* space group with four formula units per unit cell. The authors are not aware of any earlier investigation of the thermodynamic properties of the quaternary compounds Ca₂CoSi₂O₇, CaCoSiO₄, and CaCoSi₄O₁₀.

In the present study, the phase relations in the pseudoternary system CaO-CoO-SiO₂ were established for the first time by identifying the coexisting phases by X-ray diffraction (XRD) analysis and energy-dispersive analysis of X-rays (EDAX) of equilibrated samples. On the basis of the phase diagram, solid-state galvanic cells incorporating yttria-stabilized zirconia as the solid electrolyte were designed for the measurement of the Gibbs energies of formation of the stable quaternary oxides. In principle, solid-state cells based on CaF₂ as the solid electrolyte can also be employed for measuring the Gibbs energies of formation of multicomponent oxides containing Ca (Benz and Wagner 1961). However, the formation of oxyfluoride phases at the electrode-electrolyte interface can be a limitation, as discussed by Jacob (1995).

From the phase relations determined in this investigation, the mixing properties of Ca_{*x*}Co_{*1-x*}O and (Ca_{*γ*}Co_{*1-γ*})CoSiO₄ solid solutions were evaluated. A *T-X* phase diagram for the binary CaO-CoO was computed and compared with information available in the literature. The binodal and spinodal curves for the olivine solid solution (Ca_{*γ*}Co_{*1-γ*})CoSiO₄ were also derived. In addition, the chemical-potential diagrams of SiO₂, CaO, and CoO for the pseudoternary system were computed at 1323 K; these diagrams illustrate the stability field for the solid solutions and quaternary compounds.

EXPERIMENTAL METHODS

Materials

Puratronic-grade Co and Co₃O₄ powders were obtained from Johnson Matthey Chemicals Limited. Silicic acid was dehydrated at increasing temperature and fired at 1500 K for 22 h to form silica. Wollastonite (CaSiO₃) was prepared by melting an equimolar mixture of CaCO₃ and SiO₂ in a platinum container at 1950 K. The melt was quenched to form a glass and then crystallized at 1450 K to get the monoclinic phase. Formation of all the compounds was confirmed by XRD analysis.

To prepare CaCoSi₂O₆, finely divided SiO₂, Co₃O₄, and CaCO₃ were mixed in the appropriate molar ratio in a vibratory mill using agate jar and balls. The mixture was pelletized and reacted at 1600 K for a total of ~150 h. The pellets were quenched and reground to -325 mesh, repelletized, and reheated five times during this period to complete the reaction. Formation of the pink CaCoSi₂O₆ was confirmed by X-ray diffraction. The lattice parameters of CaCoSi₂O₆ obtained by XRD are $a = 0.9806(5)$, $b = 0.8952(4)$, $c = 0.5245(3)$ nm, and $\beta = 105.45(3)^\circ$, which differ significantly from those reported by White et al. (1971; $a = 0.9773$, $b = 0.8945$, $c = 0.5252$ nm, and $\beta = 105.45^\circ$), but agree with the more recent data of Ghose and Wan (1975; $a = 0.9806$, $b = 0.8950$, $c = 0.5243$ nm, and $\beta = 105.45^\circ$) and Wright and Navrotsky (1985; $a = 0.9807$, $b = 0.8952$, $c = 0.5248$ nm, and $\beta = 105.45^\circ$).

Violet-colored CaCoSiO₄ was prepared by solid-state reaction of finely ground Co₃O₄, CaCO₃, and SiO₂. Pressed pellets were calcined at 1323 K under flowing argon gas for a total of ~150 h. The pellets were quenched, ground to -325 mesh, and repelletized for heat treatment three times during this period. The lattice parameters of CaCoSiO₄, obtained by XRD, are $a = 0.4822(3)$, $b = 1.1108(6)$, and $c = 0.6406(4)$ nm, with space group *Pnma*, $Z = 4$, which are in reasonable agreement with those reported by Newnham et al. (1966; $a = 0.4827$, $b = 1.112$, and $c = 0.6422$ nm).

For the preparation of Ca₂CoSi₂O₇, finely divided SiO₂, CaCO₃, and Co₃O₄ were heated at 1473 K for up to ~100 h. Ca₂CoSi₂O₇ has a melilite structure with tetragonal space group *P4₂m*. The structure can be described as consisting of Si₂O₇ groups linked with CoO₄ tetrahedra to form corrugated sheets. The sheets are held together by large Ca²⁺ cations in distorted eightfold coordination. The lattice parameters of the compound determined by XRD are $a = 0.7841(4)$ and $c = 0.5024(3)$ nm. The value in parentheses is the uncertainty in the last digit of the number. The lattice parameters obtained in this study are more precise than those reported by Brisi and Abbattista (1960), $a = 0.786$ and $c = 0.503$ nm. The compound was also obtained by crystallization of a melt at 1523 K. On the basis of the purity of the compounds used for synthesis, the ternary and quaternary oxides prepared in this study were expected to have a purity better than 99.9%.

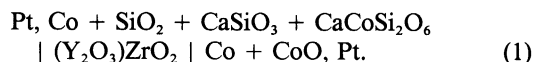
The electrode pellets were made by mixing the constituent powders in equimolar ratio, pelletizing, and sintering at 1400 K. Yttria-stabilized zirconia tubes, closed at one end, were obtained from Corning Glass. The argon gas used in the experiments was 99.999% pure; it was further dried by passing through columns containing anhydrous magnesium perchlorate and phosphorus pentoxide, and deoxidized by passing over copper at 873 K and titanium at 1173 K.

Procedure

Phase equilibria. Phase relations in the system were explored by equilibrating mixtures of different binary, ternary, and quaternary oxides in air at 1323 K in a muf-

file furnace, controlled to ± 2 K. Twenty-seven pseudo-ternary compositions were equilibrated for periods of up to 140 h. The samples were quenched in chilled mercury, ground, and repelletized twice during this period. The phase composition of the samples was found to be unaltered by further heat treatment. The phases present in quenched samples were identified by XRD analysis and optical microscopy, and their compositions were determined using EDAX. To obtain reproducible analysis using EDAX, the average grain size of the sample had to be more than ~ 25 μm . Oxides CoO, SiO₂, and CaSiO₃ of purity better than 99.99% were used as standards. The accuracy of compositions determined by EDAX was ± 0.2 mol%. In XRD analysis, CuK α radiation was used and metallic silicon was mixed with the powder sample as an internal standard. After the direction of a tie line was determined, the approach to equilibrium from a different direction was checked starting with a new set of initial compositions. In all cases, the direction of the tie line was found to be independent of the starting compounds used in preparing samples with identical bulk composition.

Thermodynamic properties. On the basis of the phase relations established in this study, a solid-state galvanic cell, using yttria-stabilized zirconia as the electrolyte, was designed for accurate measurement of the Gibbs energy of formation of CaCoSi₂O₆ (Cpx) from CoO (rock salt), SiO₂ (Qtz), and CaSiO₃ (Wol) in the temperature range of 1000–1324 K:



The cell is written such that the electrode on the right side is positive. The cell essentially measures the activity of CoO in the three-phase field CaCoSi₂O₆ + CaSiO₃ + SiO₂. Because CaO and SiO₂ are more stable than CoO, the activity of CoO was determined by equilibrating the oxide mixture with metallic Co and measuring the chemical potential of O in the system. The apparatus for electromotive force (emf) measurements, incorporating a closed-end (Y₂O₃)ZrO₂ tube, was described by Jacob et al. (1986). The Co + CoO reference electrode was prepared by compacting the powder mixture against the closed end of the tube, with a platinum lead buried in the mixture. The four-phase electrode pellet was spring loaded against the outside surface of the tube using a system of alumina slabs and rods. A platinum gauze was pressed against the electrode pellet. A platinum lead was spot welded to the gauze. Each electrode was flushed by separate purified streams of argon. This cell arrangement prevented O transport via the gas phase between the two electrodes.

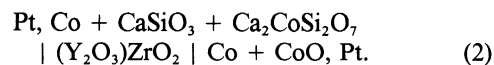
The cell assembly was enclosed in a recrystallized alumina tube fitted with brass caps on both ends. Gas inlet and outlet, and provision for insulated electrical leads, were provided on the brass caps. The alumina tube enclosing the cell was suspended inside a vertical furnace such that the electrodes were maintained in the constant temperature (± 1 K) zone. A Kanthal tape, wound around

the alumina tube, was earthed to minimize induced emf on the platinum leads from furnace windings.

The emf of the cell was measured with a high-impedance digital voltmeter in the temperature range of 1000–1324 K under argon gas at atmospheric pressure. The temperature of the cell was controlled to ± 1 K and measured by a Pt–Pt-13%Rh thermocouple calibrated against the melting point of gold. All temperature measurements refer to the ITS-90 scale. The emf of the cell registered a steady value in 3–8 h depending on temperature; longer periods were required at lower temperatures. Reversibility of the emf was checked by microcoulometric titration. A small current (~ 50 μA) was passed through the cell in either direction for ~ 5 min using an external potential source. After titration in each direction, the open-circuit emf was monitored as a function of time. In all cases, the emf was found to return to the original value before the titration, confirming reversibility. The emf was found to be reproducible when cycling temperature and was independent of the flow rate of argon gas through the cell in the range of 2–6 mL/s. To ensure the absence of thermal gradients across the cell, the emf of a symmetric cell with identical Co + CoO electrodes was measured as a function of temperature. The cell emf was ± 0.2 mV, and no systematic trends were observed. The emf of the symmetric cell should be zero under isothermal conditions. If a temperature gradient is present across the electrolyte, then it functions as a thermocell, and the emf is proportional to the temperature difference between the electrodes. When the experiments had concluded, the electrodes were examined by XRD and optical microscopy. The phase composition of the electrodes was found to be unaltered during the experiment.

Application of the phase rule to the condensed phase system CaO-CoO-SiO₂ at constant temperature and total pressure indicates that the degree of freedom is zero when three phases coexist. Two-phase equilibria are generally associated with one degree of freedom, except when special constraints apply. An example of a special constraint is seen along the two-phase join CaSiO₃-Ca₂CoSi₂O₇. Because the mole ratio of CaO to SiO₂ is unity for both phases, the degree of freedom is reduced by one. Therefore, the activity of CoO is uniquely fixed by this two-phase equilibrium at constant temperature and pressure. It follows that the chemical potential of CoO is identical in the two adjoining three-phase regions CaSiO₃ + Ca₂CoSi₂O₇ + CaCoSi₂O₆ and CaSiO₃ + Ca₂CoSi₂O₇ + Ca₃Si₂O₇. Similarly, the activity of CoO is determined uniquely by the two-phase equilibrium involving Ca₂CoSi₂O₇ and CaCoSiO₄ (see Table 1).

The solid-state galvanic cell designed for measurement of the Gibbs energy of formation of Ca₂CoSi₂O₇ from CoO and CaSiO₃ can be written as

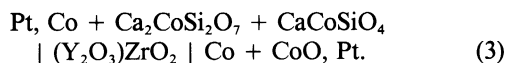


The Gibbs free energy of CaCoSiO₄ from CoO and

TABLE 1. Phase fields in the ternary system CaO-CoO-SiO₂ at 1323 K

ID no.	Phase fields
1	SiO ₂ + (Ca _Y Co _{1-Y})CoSiO ₄ , (0 ≤ Y ≤ 0.108)
2	SiO ₂ + CaCoSi ₂ O ₆ + (Ca _Y Co _{1-Y})CoSiO ₄ (Y = 0.108)
3	SiO ₂ + CaCoSi ₂ O ₆ + CaSiO ₃
4	CaCoSi ₂ O ₆ + (Ca _Y Co _{1-Y})CoSiO ₄ (0.108 ≤ Y ≤ 0.315)
5	CaCoSi ₂ O ₆ + (Ca _Y Co _{1-Y})CoSiO ₄ (Y = 0.315) + (Ca _Y Co _{1-Y})CoSiO ₄ (Y = 0.685)
6	CaCoSi ₂ O ₆ + (Ca _Y Co _{1-Y})CoSiO ₄ , (0.685 ≤ Y ≤ 0.870)
7	Ca ₂ CoSi ₂ O ₇ + (Ca _Y Co _{1-Y})CoSiO ₄ , (0.87 ≤ Y ≤ 1)
8	CaCoSi ₂ O ₆ + Ca ₂ CoSi ₂ O ₇ + (Ca _Y Co _{1-Y})CoSiO ₄ , (Y = 0.870)
9	CaCoSi ₂ O ₆ + CaSiO ₃ + Ca ₂ CoSi ₂ O ₇
10	Ca ₂ CoSi ₂ O ₇ + CaSiO ₃ + Ca ₃ Si ₂ O ₇
11	Ca ₂ CoSi ₂ O ₇ + CaCoSiO ₄ + Ca ₃ Si ₂ O ₇
12	CoO + (Ca _Y Co _{1-Y})CoSiO ₄ , (0 ≤ Y ≤ 0.315)
13	CoO + (Ca _Y Co _{1-Y})CoSiO ₄ (Y = 0.315) + (Ca _Y Co _{1-Y})CoSiO ₄ (Y = 0.685)
14	CoO + (Ca _Y Co _{1-Y})CoSiO ₄ , (0.685 ≤ Y ≤ 1)
15	CoO + CaCoSiO ₄ + Ca ₃ Si ₂ O ₇
16	CoO + Ca ₃ Si ₂ O ₇ + Ca ₂ SiO ₄
17	Ca ₂ SiO ₄ + Ca _X Co _{1-X} O, (0 ≤ X ≤ 0.142)
18	Ca ₂ SiO ₄ + Ca _X Co _{1-X} O (X = 0.142) + Ca _Y Co _{1-Y} O (X = 0.917)
19	Ca ₂ SiO ₄ + Ca _X Co _{1-X} O, (0.917 ≤ X ≤ 1)

Ca₂CoSi₂O₇ was measured using the solid-state cell represented as



For Cells 2 and 3, emf measurements were performed following the same procedure as that used for Cell 1.

RESULTS AND DISCUSSION

Phase equilibria

The equilibrium phase diagram for the pseudoternary system CaO-CoO-SiO₂ at 1323 K, deduced from the results of this study, is shown in Figure 1. Only one compound, Co₂SiO₄, was found along the pseudobinary CoO-SiO₂, whereas three compounds, Ca₂SiO₄, Ca₃Si₂O₇, and CaSiO₃, were found on the CaO-SiO₂ join. Inside the ternary system, three quaternary compounds, CaCoSi₂O₆, Ca₂CoSi₂O₇, and CaCoSiO₄, were observed. The compound CaCoSi₂O₆ appears to be nonstoichiometric, containing up to 2.5 mol% excess CoSiO₃. Essentially pure CoO coexists with Ca₂SiO₄, Ca₃Si₂O₇, and the solid solution (Ca_YCo_{1-Y})CoSiO₄. Ca-rich and Ca-poor phases of the Ca_XCo_{1-X}O solid solution with the NaCl structure coexist only with Ca₂SiO₄. There is a small solubility of ~2 mol% of Co₂SiO₄ in Ca₂SiO₄. There was no evidence for the existence of the compound CaCoSi₄O₁₀ reported by Nicolini and Porta (1970). Their XRD pattern for CaCoSi₄O₁₀ corresponds to the phase mixture of CaCoSi₂O₆ and SiO₂. Ca_XCo_{1-X}O and (Ca_YCo_{1-Y})CoSiO₄ solid solutions exist with miscibility gaps extending from X = 0.142–0.917 and Y = 0.315–0.685, respectively. The solid solution with olivine structure terminates at the composition CaCoSiO₄. Because the M2 sites in the olivine structure are larger than M1 sites, Ca²⁺ ions probably substitute for Co²⁺ ions only on M2; thus, the

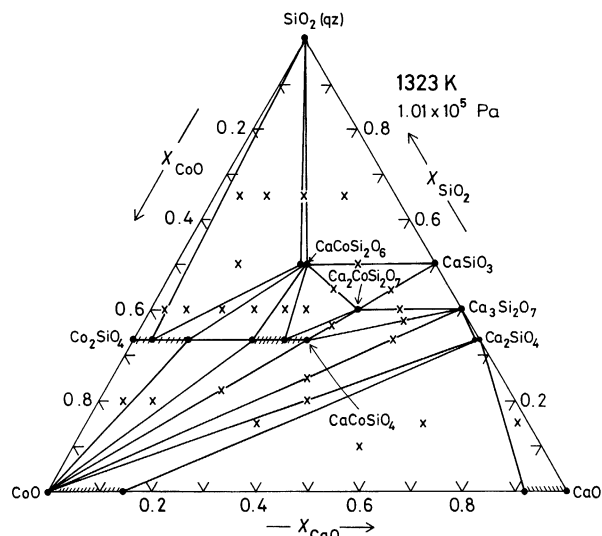


FIGURE 1. Phase relations in the system CaO-CoO-SiO₂ at 1323 K. The bulk compositions of the equilibrated samples are shown by Xs.

limit of the olivine solid solution is at the composition CaCoSiO₄. Hence, the solid solution may be represented as (Ca_YCo_{1-Y})_{M2}(Co)_{M1}SiO₄. There are 11 phase fields in which three condensed phases coexist, and ten phase fields in which a solid solution coexists with a condensed phase. Phase relations were not explored at lower temperatures because of the prohibitively long equilibration periods involved.

Gibbs energies of formation of the quaternary compounds

Gibbs energy of formation of CaCoSi₂O₆. The reversible emf of Cell 1, E_1 , is plotted as a function of temperature in Figure 2. Within the accuracy of measurement, ± 0.7 mV and ± 1 K, emf is a linear function of temperature. This suggests that phase relations established at 1323 K are valid over the entire temperature range of emf measurement. Least-squares regression analysis of the emf of Cell 1 gives

$$E_1 = 144.5 - 6.15 \times 10^{-2} T (\pm 0.7) \text{ mV} \quad (4)$$

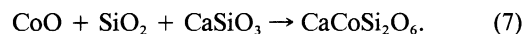
The uncertainty limit is based on twice the standard error estimate. The O chemical potential at the right electrode of Cell 1 is determined by the reaction



At the left electrode, the O potential is fixed by the equilibrium between the four condensed phases:



The overall cell reaction is



The standard Gibbs energy of formation of CaCoSi₂O₆ according to Reaction 7, $\Delta G_{f,7}^0$, is obtained directly from the emf:

$$\begin{aligned}\Delta G_{f,7}^0 &= -nFE_1 \\ &= -27890 + 11.87T (\pm 135) \text{ J/mol}\end{aligned}\quad (8)$$

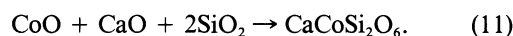
where $n = 2$ is the number of electrons involved in electrochemical reactions at each electrode, F is the Faraday constant, and E_1 is the emf of Cell 1.

The Gibbs energy of formation of the quaternary oxide from component binary oxides can be derived using the free energy of formation of CaSiO_3 reported earlier (Mukhopadhyay and Jacob 1995):



$$\Delta G_{f,9}^0 = -90030 - 0.61T (\pm 60) \text{ J/mol.} \quad (10)$$

The combination of Equations 7 and 9 gives



The corresponding standard Gibbs free energy of formation of $\text{CaCoSi}_2\text{O}_6$ from component binary oxides is

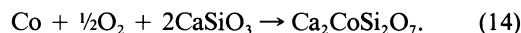
$$\Delta G_{f,11}^0 = -117920 + 11.26T (\pm 150) \text{ J/mol.} \quad (12)$$

The temperature-independent term in Equation 12 gives the enthalpy change for Reaction 11 at a mean experimental temperature of 1162 K. The enthalpy of formation of $\text{CaCoSi}_2\text{O}_6$ from CoO , SiO_2 , and CaO is $-117.9 (\pm 1)$ kJ/mol. This second law enthalpy of formation of $\text{CaCoSi}_2\text{O}_6$ from component binary oxides is in fair agreement with the results obtained by Navrotsky and Coons (1976) [$\Delta H_{f,11}^0 = -111.7 (\pm 2)$ kJ/mol at 986 K] using oxide-melt solution calorimetry. The entropy change for Reaction 11 is $-11.26 (\pm 0.86)$ J/(K·mol) at 1162 K. Unfortunately, systematic studies of the heat capacity of $\text{CaCoSi}_2\text{O}_6$ as a function of temperature have not been reported in the literature.

Gibbs energy of formation of $\text{Ca}_2\text{CoSi}_2\text{O}_7$. The reversible emf of Cell 2, E_2 , is also plotted as a function of temperature in Figure 2. Least-squares regression analysis gives

$$E_2 = 65.4 - 1.86 \times 10^{-2}T (\pm 0.5) \text{ mV.} \quad (13)$$

The O chemical potential at the right electrode of Cell 2 is the same as that in Cell 1 and is determined by Reaction 5. At the left electrode, the O potential is fixed by the equilibrium between the three condensed phases, which exist at unit activity,



The overall cell reaction is



The standard Gibbs energy of formation of the quaternary oxide from CoO and CaSiO_3 is obtained directly from the emf:

$$\begin{aligned}\Delta G_{f,15}^0 &= -nFE_2 \\ &= -12630 + 3.60T (\pm 100) \text{ J/mol.}\end{aligned}\quad (16)$$

Gibbs energy of formation of the quaternary oxide from

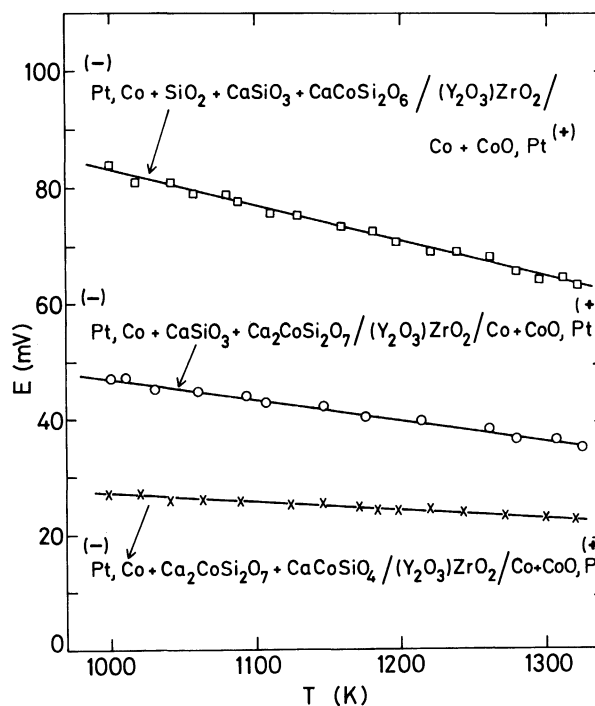


FIGURE 2. Temperature dependence of the emf of cells 1, 2, and 3, incorporating $(\text{Y}_2\text{O}_3)\text{ZrO}_2$ as the solid electrolyte.

component binary oxides can be derived using the free energy of formation of CaSiO_3 . The combination of Equations 9 and 15 gives

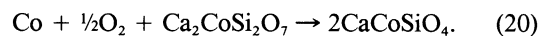


$$\begin{aligned}\Delta G_{f,17}^0 &= -192690 \\ &+ 2.38T (\pm 130) \text{ J/mol.}\end{aligned}\quad (18)$$

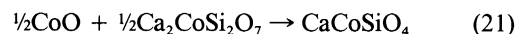
Gibbs energy of formation of CaCoSiO_4 . The reversible emf of Cell 3, E_3 , is plotted as a linear function of temperature in Figure 2. Least-squares regression analysis gives

$$E_3 = 41.2 - 1.41 \times 10^{-2}T (\pm 0.4) \text{ mV.} \quad (19)$$

At the left electrode, the O potential is fixed by the equilibrium between the three condensed phases, each at unit activity,



The standard free energy of formation of the compound CaCoSiO_4 from CoO and $\text{Ca}_2\text{CoSi}_2\text{O}_7$,



is obtained directly from the emf:

$$\Delta G_{f,21}^0 = -FE_3 = -3980 + 1.36T (\pm 40) \text{ J/mol.} \quad (22)$$

The Gibbs energy of formation of the quaternary oxide from component binary oxides can be derived using the free energy of formation of $\text{Ca}_2\text{CoSi}_2\text{O}_7$, determined in this study. The combination of Equations 17 and 21 gives

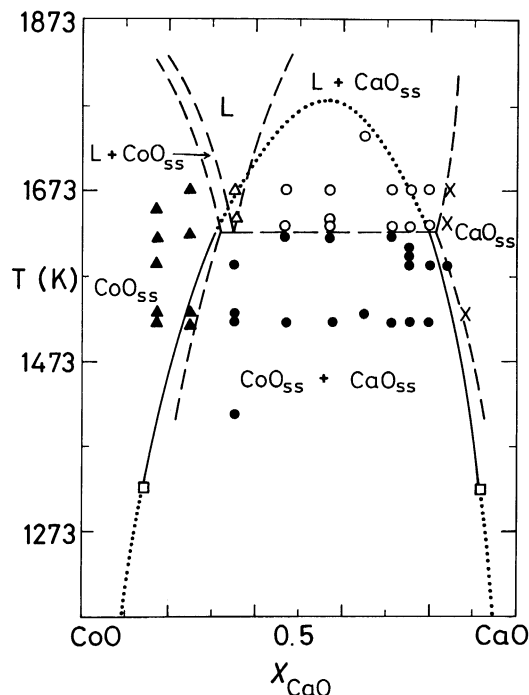


FIGURE 3. Phase-equilibrium diagram for the system CaO-CoO. Separate symbols are used for each phase assemblage. The solid triangles, Xs, solid circles, open triangles, and open circles represent CoO_{ss}, CaO_{ss}, CaO_{ss} + CoO_{ss}, liquid, and CaO_{ss} + liquid phase fields, respectively (Woermann and Muan 1970). Dashed lines represent the phase boundaries suggested by Woermann and Muan. Experimental points from the present study are indicated by open squares. Continuous and dotted lines are computed on the basis of subregular solution parameters deduced in this study.



for which,

$$\Delta G_{f,23}^0 = -100325 + 2.55T (\pm 100) \text{ J/mol.} \quad (24)$$

The standard Gibbs energies of formation of the silicates from elements can be readily derived by combining their free energies of formation from oxides obtained in this study with data on binary oxides given in standard tables.

Mixing properties of the solid solutions at 1323 K

Ca_xCo_{1-x}O solid solution. The mixing properties of Ca_xCo_{1-x}O solid solution can be determined from the miscibility gap. The region of immiscibility at 1323 K extends from $X = 0.142$ to 0.917 . Because the two compositions are not symmetric, a subregular solution model may be used to describe the system (Hardy 1953). The activities of the end-members are given by

$$a_{\text{CaO}} = X \exp\{(1 - X)^2[(2A - B)X + B(1 - X)]/RT\} \quad (25)$$

$$a_{\text{CoO}} = (1 - X) \exp\{X^2[(2B - A)(1 - X) + AX]/RT\}. \quad (26)$$

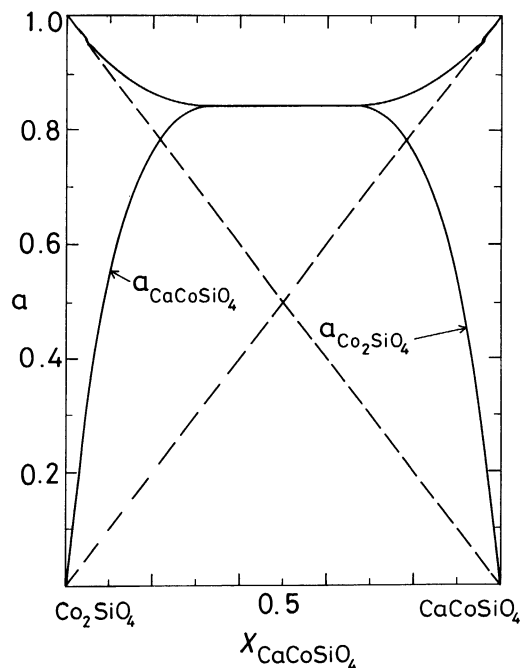


FIGURE 4. Activity-composition relations for the olivine solid solution (Ca_yCo_{1-y})CoSiO₄ at 1323 K.

Within the region of unmixing ($0.142 \leq X \leq 0.917$ at 1323 K), the activities of CaO and CoO are constant. The subregular solution model constants A and B were determined at 1323 K by solving the equations

$$a_{\text{CaO}}|_{X=0.142} = a_{\text{CaO}}|_{X=0.917} \quad (27)$$

$$a_{\text{CoO}}|_{X=0.142} = a_{\text{CoO}}|_{X=0.917} \quad (28)$$

where the activities are defined by Equations 25 and 26. The integral excess free energy for Ca_xCo_{1-x}O solid solution can be expressed as

$$\begin{aligned} \Delta G^E &= X(1 - X)[AX + B(1 - X)] \\ &= X(1 - X)[31975X + 26736(1 - X)] \text{ J/mol.} \end{aligned} \quad (29)$$

On the basis of this equation, the miscibility gap was computed as a function of temperature using the procedure outlined by Oonk (1981), assuming ideal mixing of cations. The critical temperature and composition for the closure of the miscibility gap are $T = 1780$ K and $X = 0.573$, respectively.

The phase equilibria in the system CaO-CoO in air were determined by Woermann and Muan (1970) from 1093 to 1300 K and 1410 to 1740 K. Specific CaO/CoO ratios were held at temperature sufficiently long for attainment of equilibrium and then quenched rapidly to room temperature. Phases present were determined by microscopic and X-ray examination. The minimum in their liquidus curve indicates a miscibility gap in the subsolidus region, which is supported by the disparity in the six coordinated ionic radii between Ca²⁺ and Co²⁺ [0.1000 nm (Shannon and Prewitt 1969) and 0.0745 nm (Shannon and Prewitt 1970), respectively]. The experimental

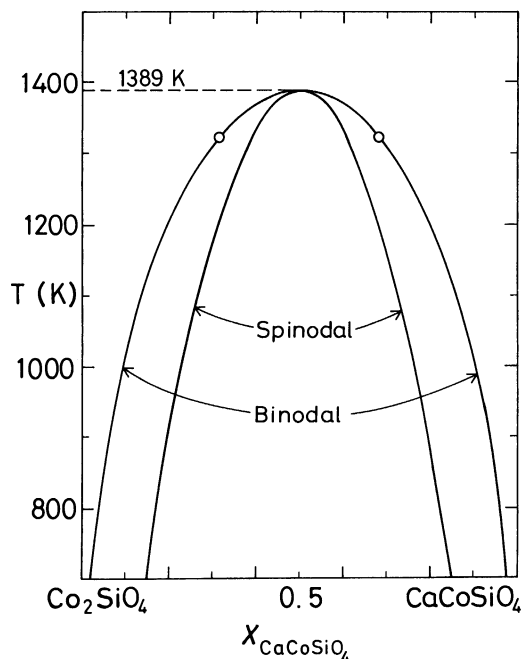


FIGURE 5. Computed binodal and spinodal curves for the olivine solid solution $(\text{Ca}_y\text{Co}_{1-y})\text{CoSiO}_4$.

T - X phase diagram determined by Woermann and Muan (1970) is compared with the computed immiscibility in Figure 3.

Although the width of the immiscible region is approximately the same in both studies, the results of this study suggest a lateral displacement of the region toward the CoO side by 2–4 mol%. Recent studies (Jacob and Varghese 1995) of solid solutions with NaCl structures in the system BaO-SrO suggest a small positive excess entropy of mixing, $\Delta S^E = \Delta H^E/4710$. Presence of excess entropy causes mild progressive enlargement of the immiscible region with decreasing temperature below 1323 K in the system CaO-CoO. The computed miscibility gap contracts slightly above the experimental temperature. Comparison of the phase boundaries obtained in this study with those of Woermann and Muan (1970) indicates that excess entropy and resulting contraction of the gap at high temperature is negligible.

$(\text{Ca}_y\text{Co}_{1-y})\text{CoSiO}_4$ solid solution. The mixing properties of the $(\text{Ca}_y\text{Co}_{1-y})\text{CoSiO}_4$ solid solution were determined from the limits of miscibility along the pseudobinary CaCoSiO_4 - Co_2SiO_4 , following a procedure similar to that used above. As the region of demixing is symmetric about $Y = 0.5$, a regular-solution model was employed to express the mixing properties. The expressions for the activities of the end-members in a regular solution are

$$a_{\text{CaCoSiO}_4} = Y \exp[\Omega(1 - Y)^2/RT] \quad (30)$$

$$a_{\text{Co}_2\text{SiO}_4} = (1 - Y) \exp(\Omega Y^2/RT) \quad (31)$$

where Ω is the constant of the regular-solution model. The value of the constant was calculated from the phase-

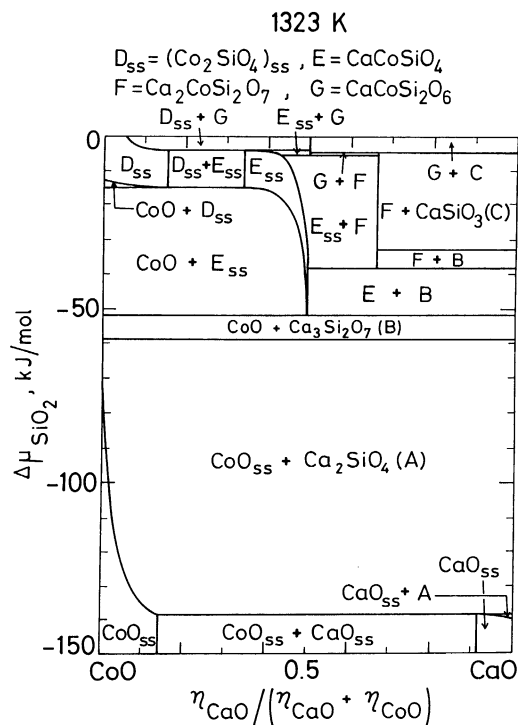


FIGURE 6. Chemical potential of SiO_2 relative to quartz as a function of normalized mole fraction in the pseudoternary system CaO-CoO-SiO₂ at 1323 K.

boundary compositions $Y = 0.315$ and 0.685 at 1323 K. The integral excess free energy of mixing of the solid solution can be expressed as

$$\Delta G^E = 23100 (\pm 250) Y(1 - Y) \text{ J/mol.} \quad (32)$$

The cations are assumed to mix randomly on the M2 sites of the olivine structure. The activities of Co_2SiO_4 and CaCoSiO_4 at 1323 K exhibit large positive deviation from Raoult's law (Fig. 4). In the region of unmixing, activity of each component is 0.844. The calculated binodal and spinodal curves are shown in Figure 5. The excess free energy is assumed to be independent of temperature. The chemical spinodal curve is the locus of points along which $(\partial^2 G/\partial Y^2) = 0$. Phase separation occurs spontaneously without an activation barrier inside the spinodal region. In the region between the binodal and spinodal curves, phase separation is sluggish. The calculated critical temperature is $1389 (\pm 15)$ K. The immiscibility is caused by the difference between the ionic radii of Ca^{2+} and Co^{2+} . It is interesting to note that Mukhopadhyay and Lindsley (1983) observed an approximately symmetric miscibility gap in the subsolidus region of the pseudobinary system CaFeSiO_4 - Fe_2SiO_4 below 1313 K.

Chemical-potential diagrams

For providing an insight into the stability domain of different phases, the chemical potential of any one of the components in a pseudoternary system can be depicted in two dimensions as a function of the normalized mole

TABLE 2. Reactions defining the chemical potential of SiO₂ in different phase fields at 1323 K

Phase fields	Reactions defining chemical potential of SiO ₂
1-3	In equilibrium with pure SiO ₂ ($\Delta\mu_{\text{SiO}_2} = 0$)
4-6, 8	$(\text{CaCoSiO}_4)_{\text{ss}} + \text{SiO}_2 \rightarrow \text{CaCoSi}_2\text{O}_6$
7, 8	$4(\text{CaCoSiO}_4)_{\text{ss}} + \text{SiO}_2 \rightarrow 2\text{Ca}_2\text{CoSi}_2\text{O}_7 + (\text{Co}_2\text{SiO}_4)_{\text{ss}}$
9	$\text{Ca}_2\text{CoSi}_2\text{O}_7 + \text{SiO}_2 \rightarrow \text{CaCoSi}_2\text{O}_6 + \text{CaSiO}_3$
10	$\text{Ca}_3\text{Si}_2\text{O}_7 + \text{SiO}_2 \rightarrow 3\text{CaSiO}_3$
11	$3\text{CaCoSiO}_4 + \text{Ca}_3\text{Si}_2\text{O}_7 + \text{SiO}_2 \rightarrow 3\text{Ca}_2\text{CoSi}_2\text{O}_7$
12-14	$2\text{CoO} + \text{SiO}_2 \rightarrow (\text{Co}_2\text{SiO}_4)_{\text{ss}}$
15	$3\text{CoO} + \text{Ca}_3\text{Si}_2\text{O}_7 + \text{SiO}_2 \rightarrow 3\text{CaCoSiO}_4$
16	$3\text{Ca}_2\text{SiO}_4 + \text{SiO}_2 \rightarrow 2\text{Ca}_3\text{Si}_2\text{O}_7$
17-19	$2(\text{CaO})_{\text{ss}} + \text{SiO}_2 \rightarrow \text{Ca}_2\text{SiO}_4$

fraction of the other two components at constant temperature. The composition of a component is normally designated by its mole fraction, which is obtained by dividing the number of moles of the component with the sum of moles of all components. The normalized mole fraction, used as a composition variable in the chemical-potential diagrams, is obtained by removing the component, the chemical potential of which is being plotted, from the summation. Thus, the chemical potential becomes an independent variable with respect to the normalized mole fraction. The topology of this representation is equivalent to the more familiar temperature-composition diagrams for pseudobinary systems at constant pressure. The chemical-potential regimes for the existence of different phases or phase mixtures can be readily read from the diagram. If experimental data are plotted in this manner, many inconsistencies in thermodynamic description, which are not self evident, become obvious. Inconsistent data lead to constructions that violate topological rules.

The variation of the chemical potential of SiO₂ with the normalized mole fraction $\eta_{\text{CaO}}/(\eta_{\text{CaO}} + \eta_{\text{CoO}})$ in the pseudoternary system CaO-CoO-SiO₂ at 1323 K is shown in Figure 6. The variation of the chemical potential of SiO₂, relative to quartz as the standard state, was calculated using the Gibbs energies of formation of the quaternary compounds and the mixing properties of the solid solutions determined in the present study, as well as the thermodynamic information on the binary system CaO-

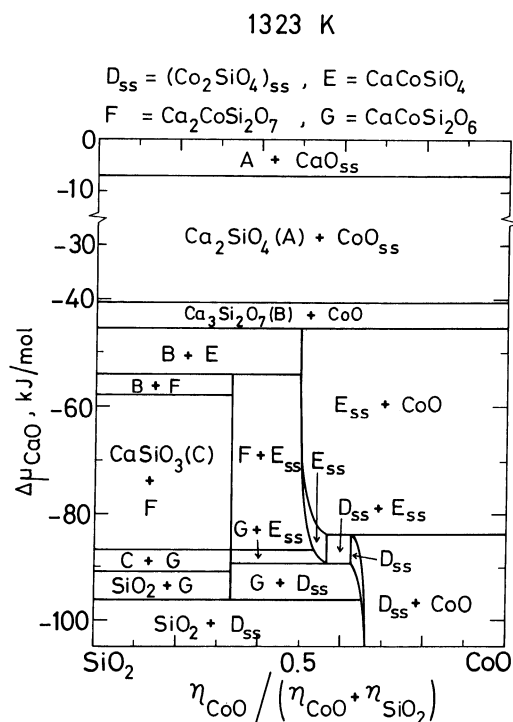
TABLE 3. Reactions defining the chemical potential of CaO in different phase fields at 1323 K

Phase fields	Reactions defining chemical potential of CaO
1, 2	$(\text{Co}_2\text{SiO}_4)_{\text{ss}} + \text{SiO}_2 + 2\text{CaO} \rightarrow 2(\text{CaCoSiO}_4)_{\text{ss}}$
3	$\text{SiO}_2 + \text{CaO} \rightarrow \text{CaSiO}_3$
2, 4-6	$(\text{Co}_2\text{SiO}_4)_{\text{ss}} + \text{CaCoSi}_2\text{O}_6 + 2\text{CaO} \rightarrow 3(\text{CaCoSiO}_4)_{\text{ss}}$
7	$(\text{Co}_2\text{SiO}_4)_{\text{ss}} + \text{Ca}_2\text{CoSi}_2\text{O}_7 + \text{CaO} \rightarrow 3(\text{CaCoSiO}_4)_{\text{ss}}$
8, 9	$\text{CaCoSi}_2\text{O}_6 + \text{CaO} \rightarrow \text{Ca}_2\text{CoSi}_2\text{O}_7$
10	$2\text{CaSiO}_3 + \text{CaO} \rightarrow \text{Ca}_3\text{Si}_2\text{O}_7$
11	$2\text{Ca}_2\text{CoSi}_2\text{O}_7 + \text{CaO} \rightarrow 2\text{CaCoSiO}_4 + \text{Ca}_3\text{Si}_2\text{O}_7$
12-14	$(\text{Co}_2\text{SiO}_4)_{\text{ss}} + \text{CaO} \rightarrow (\text{CaCoSiO}_4)_{\text{ss}} + \text{CoO}$
15	$2\text{CaCoSiO}_4 + \text{CaO} \rightarrow \text{Ca}_3\text{Si}_2\text{O}_7 + 2\text{CoO}$
16	$\text{Ca}_3\text{Si}_2\text{O}_7 + \text{CaO} \rightarrow 2\text{Ca}_2\text{SiO}_4$
17-19	Fixed by the chemical potential of CaO in the solid solution $\text{Ca}_x\text{Co}_{1-x}\text{O}$

TABLE 4. Reactions defining the chemical potential of CoO in different phase fields at 1323 K

Phase fields	Reactions defining chemical potential of CoO
1, 2	$\text{SiO}_2 + 2\text{CoO} \rightarrow (\text{Co}_2\text{SiO}_4)_{\text{ss}}$
3	$\text{CaSiO}_3 + \text{SiO}_2 + \text{CoO} \rightarrow \text{CaCoSi}_2\text{O}_6$
2, 4-6, 8	$\text{CaCoSi}_2\text{O}_6 + 2\text{CoO} \rightarrow (\text{Co}_2\text{SiO}_4)_{\text{ss}} + (\text{CaCoSiO}_4)_{\text{ss}}$
7, 8	$\text{Ca}_2\text{CoSi}_2\text{O}_7 + \text{CoO} \rightarrow 2(\text{CaCoSiO}_4)_{\text{ss}}$
9, 10	$2\text{CaSiO}_3 + \text{CoO} \rightarrow \text{Ca}_2\text{CoSi}_2\text{O}_7$
11	$\text{Ca}_2\text{CoSi}_2\text{O}_7 + \text{CoO} \rightarrow 2\text{CaCoSiO}_4$
12-16	In equilibrium with pure CoO ($\Delta\mu_{\text{CoO}} = 0$)
17-19	Fixed by the chemical potential of CoO in the solid solution $\text{Ca}_x\text{Co}_{1-x}\text{O}$

SiO₂ (Hillert et al. 1990, 1991) and Co₂SiO₄ (Kale and Jacob 1989). In the calculation, the small solid solubilities associated with phases CaCoSi₂O₆ and Ca₂SiO₄ were ignored. When three condensed phases coexist at constant temperature and pressure, the silica chemical potential is invariant and can be represented by a horizontal line. The chemical potential of SiO₂ is a variable in the two-phase fields. For phase fields involving a pure condensed phase and a solid solution [$\text{Ca}_x\text{Co}_{1-x}\text{O} + \text{Ca}_2\text{SiO}_4$, $\text{CoO} + (\text{Ca}_y\text{Co}_{1-y})\text{CoSiO}_4$, $\text{CaCoSi}_2\text{O}_6 + (\text{Ca}_y\text{Co}_{1-y})\text{CoSiO}_4$, and $\text{Ca}_2\text{CoSi}_2\text{O}_7 + (\text{Ca}_y\text{Co}_{1-y})\text{CoSiO}_4$], the curved boundary can be obtained from the reactions that fix the chemical potential of silica (Tables 1 and 2). The chemical potential of SiO₂ in phase fields containing pure quartz is zero.

**FIGURE 7.** Chemical potential of CaO relative to pure CaO as a function of normalized mole fraction in the pseudoternary system CaO-CoO-SiO₂ at 1323 K.

Similarly, the reactions fixing the chemical potentials of CaO and CoO for different two- and three-phase equilibria are listed in Tables 3 and 4, respectively. The variation of the chemical potential of CaO with the normalized mole fraction is depicted in Figure 7. The chemical potential of CaO in the three-phase region $\text{Ca}_x\text{Co}_{1-x}\text{O}$ ($X = 0.142$) + Ca_2SiO_4 + $\text{Ca}_x\text{Co}_{1-x}\text{O}$ ($X = 0.917$) is fixed only by the mixing properties of the monoxide solid solution. The two-phase fields Ca_2SiO_4 + $\text{Ca}_x\text{Co}_{1-x}\text{O}$ ($0.917 \leq X \leq 1$) and Ca_2SiO_4 + $\text{Ca}_x\text{Co}_{1-x}\text{O}$ ($0 \leq X \leq 0.142$) exist above and below the horizontal line corresponding to the three-phase field. The two-phase equilibria involving $\text{CaCoSi}_2\text{O}_6$ and $\text{Ca}_2\text{CoSi}_2\text{O}_7$ uniquely define the chemical potential of CaO because the mole ratio of SiO₂ to CoO is two for both compounds. Consequently, the chemical potential of CaO is identical in the three-phase fields $\text{CaCoSi}_2\text{O}_6$ + $\text{Ca}_2\text{CoSi}_2\text{O}_7$ + CaSiO_3 and $\text{CaCoSi}_2\text{O}_6$ + $\text{Ca}_2\text{CoSi}_2\text{O}_7$ + $(\text{Ca}_x\text{Co}_{1-x})\text{CoSiO}_4$ ($Y = 0.87$) at constant temperature and pressure.

The chemical potential for CoO is the same in the three-phase fields $\text{CaCoSi}_2\text{O}_6$ + $\text{Ca}_2\text{CoSi}_2\text{O}_7$ + CaSiO_3 and $\text{Ca}_2\text{CoSi}_2\text{O}_7$ + $\text{Ca}_3\text{Si}_2\text{O}_7$ + CaSiO_3 (Fig. 8). Except when solid-solution phases are involved, the two-phase fields are bounded by horizontal and vertical lines. If the O potential over the condensed phases in the system CaO-CoO-SiO₂ were lowered, there would be selective reduction of CoO in solid solution or in ternary or quaternary

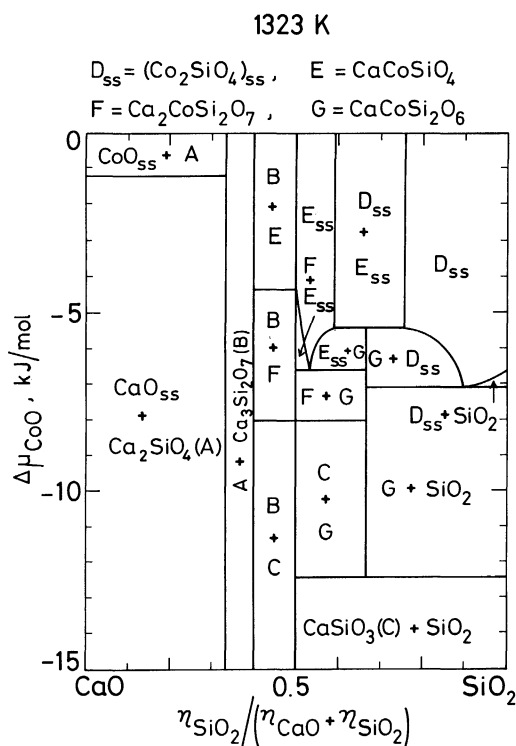


FIGURE 8. Chemical potential of CoO relative to pure CoO as a function of normalized mole fraction in the pseudoternary system CaO-CoO-SiO₂ at 1323 K.

compounds. The critical O potential for the precipitation of metallic cobalt at 1323 K for any composition can be computed from the relative chemical potential of CoO ($\Delta\mu_{\text{CoO}} = RT \ln a_{\text{CoO}}$) given in Figure 8 and the standard free energy of formation of CoO. Phase relations and chemical-potential diagrams at other temperatures can be readily computed from the thermodynamic information obtained in this study.

ACKNOWLEDGMENTS

S.M. wishes to thank the Council of Scientific and Industrial Research (India), for financial support.

REFERENCES CITED

- Benz, R., and Wagner, C. (1961) Thermodynamics of the solid system CaO-SiO₂ from electromotive force data. *Journal of Physical Chemistry*, 65, 1308-1311.
- Brisi, C., and Abbattista, F. (1960) Silicates with a melilite structure containing cobalt. *Annali de Chimica (Rome)*, 50, 1435-1437.
- Ghose, S., and Wan, C. (1975) Crystal structures of $\text{CaCoSi}_2\text{O}_6$ and $\text{CaNiSi}_2\text{O}_6$: Crystal chemical relations in $C2/c$ pyroxenes. *Eos*, 56, 1076.
- Ghose, S., Wan, C., and Okamura, F.P. (1987) Crystal structures of $\text{CaNiSi}_2\text{O}_6$ and $\text{CaCoSi}_2\text{O}_6$ and some crystal-chemical relations in $C2/c$ clinopyroxenes. *American Mineralogist*, 72, 375-381.
- Hardy, H.K. (1953) A "sub-regular" solution model and its application to some binary alloy systems. *Acta Metallurgica*, 1, 202-209.
- Hillert, M., Sundman, B., and Wang, X. (1990) An assessment of the CaO-SiO₂ system. *Metallurgical Transactions*, 21B, 303-312.
- Hillert, M., Sundman, B., Wang, X., and Barry, T. (1991) A reevaluation of the rankinite phase in the CaO-SiO₂ system. *CALPHAD*, 15, 53-58.
- Ishikawa, T., Sato, H., Kikuchi, R., and Akbar, S.A. (1985) Demixing of materials under chemical potential gradients. *Journal of the American Ceramic Society*, 68, 1-6.
- Jacob, K.T. (1983) Decomposition of β -alumina in an oxygen potential gradient. *Journal of Applied Electrochemistry*, 13, 469-472.
- (1995) Gibbs free energy of $\text{Ca}_3\text{Si}_2\text{O}_7$: A reassessment of electromotive force measurements. *Metallurgical and Materials Transactions B*, 26B, 658-660.
- Jacob, K.T., Kale, G.M., Ramachandran, A., and Shukla, A.K. (1986) Gibbs energy of formation of nickel orthosilicate (Ni_2SiO_4). *High Temperature Materials and Processes*, 7, 141-148.
- Jacob, K.T., and Shukla, A.K. (1987) Kinetic decomposition of Ni_2SiO_4 in oxygen potential gradients. *Journal of Materials Research*, 2, 338-344.
- Jacob, K.T., and Varghese, V. (1995) Solid state miscibility gap and thermodynamics of the system BaO-SrO. *Journal of Materials Chemistry*, 5, 1059-1062.
- Kale, G.M., and Jacob, K.T. (1989) Gibbs energy of formation of Co_2SiO_4 and phase relations in the system Co-Si-O. *Transactions of the Institute of Mining and Metallurgy (London)*, 98, C117-122.
- Mukhopadhyay, D.K., and Lindsley, D.H. (1983) Phase relations in the join kirschsteinite (CaFeSiO_4)-fayalite (Fe_2SiO_4). *American Mineralogist*, 68, 1089-1094.
- Mukhopadhyay, S., and Jacob, K.T. (1995) Phase equilibria in the system NiO-CaO-SiO₂ and Gibbs energy of formation of $\text{CaNiSi}_2\text{O}_6$. *Metallurgical and Materials Transactions*, 26A, 2311-2315.
- Navrotsky, A., and Coons, W.E. (1976) Thermochemistry of some pyroxenes and related compounds. *Geochimica et Cosmochimica Acta*, 40, 1281-1288.
- Newnham, R.E., Caron, L.G., and Santoro, R.P. (1966) Magnetic properties of CaCoSiO_4 and CaFeSiO_4 . *Journal of the American Ceramic Society*, 49, 284-285.
- Nicolini, L., and Porta, P. (1970) Preparation, X-ray and magnetic investigations of some silicates containing transition metal ions. *Gazzetta Chimica Italiana*, 100, 923-930.
- Onk, H.A.J. (1981) Phase theory: Thermodynamics of heterogeneous equilibria, p. 83-89. Elsevier, Amsterdam.

- Schmalzried, H., Laqua, W., and Lin, P.L. (1979) Crystalline oxide solid solutions in oxygen potential gradients. *Zeitschrift für Naturforschung*, part A, 34, 192-199.
- Shannon, R.D., and Prewitt, C.T. (1969) Effective ionic radii in oxides and fluorides. *Acta Crystallographica*, B25, 925-945.
- (1970) Revised values of effective ionic radii. *Acta Crystallographica*, B26, 1046-1048.
- Shukla, A.K., and Jacob, K.T. (1987) Kinetic instability of multicomponent solids in generalized thermodynamic gradients. *Reviews of Solid State Science*, 1, 35-53.
- White, W.B., McCarthy, G.J., and Scheetz, B.E. (1971) Optical spectra of chromium, nickel, and cobalt-containing pyroxenes. *American Mineralogist*, 56, 72-89.
- Woermann, E., and Muan, A. (1970) Phase equilibria in the system CaO-cobalt oxide in air. *Journal of Inorganic and Nuclear Chemistry*, 32, 1455-1459.
- Wright, D.P., and Navrotsky, A. (1985) A thermochemical study of the distribution of cobalt and nickel between diopsidic pyroxene and melt. *Geochimica et Cosmochimica Acta*, 49, 2385-2393.

MANUSCRIPT RECEIVED MAY 16, 1995

MANUSCRIPT ACCEPTED MARCH 4, 1996